DRAFT VERSION APRIL 5, 2023
Typeset using LATEX **twocolumn** style in AASTeX63

ASTROPHYSICAL PARAMETER INFERENCE ON ACCRETING WHITE DWARF BINARIES USING GRAVITATIONAL WAVES

SOPHIA YI,[1] KENT YAGI,[1] PHIL ARRAS,[2] AND SHU YAN LAU[1]

[1]*Department of Physics, University of Virginia, Charlottesville, VA 22904, USA.*
[2]*Department of Astronomy, University of Virginia, Charlottesville, VA 22904, USA.*

ABSTRACT

Accreting binary white dwarf systems are among the sources expected to emanate gravitational waves that will be detectable by the Laser Interferometer Space Antenna (LISA). We investigate how well we will be able to determine astrophysical parameters of accreting binary white dwarf systems from LISA's measurements of the gravitational waves emanated by these binaries. We present expressions for the gravitational wave amplitude, frequency, and frequency derivative in terms of white dwarf parameters (masses, donor radius, etc.), which we derive using knowledge of mass accreting mechanisms for binaries containing low-mass donors. We then perform a Fisher analysis to reveal the accuracy of our measurements of these parameters, relying on models from Modules for Experiments in Stellar Astrophysics (MESA) to obtain realistic mass-radius relations. We find that with an independent measurement of the luminosity distance, we are likely to be able to determine the individual masses, donor radius, and a parameter describing the response of the donor to mass loss. Without an independent measurement of the luminosity distance, we can still use LISA's measurements to determine the latter two parameters, but we are no longer able to constrain the individual masses.

1. INTRODUCTION

The first direct detection of gravitational waves (GWs) in 2015 came from the merger of a binary black hole (Abbott et al. 2016). Since then, the LIGO/Virgo Collaborations have additionally detected GW signals from numerous other binary black hole mergers, as well as several binary neutron star and neutron star-black hole mergers (Abbott et al. 2017, 2019, 2021). While LIGO and other ground-based detectors are able to detect GWs with frequencies from about 15 Hz to several kHz (Abbott et al. 2019), the Laser Interferometer Space Antenna (LISA) is a space-based GW detector expected to launch in the mid-2030s with the ability to detect GWs in the frequency range of $\sim 10^{-4}$ to 10^{-1}Hz. (Amaro-Seoane et al. 2017). Among the astrophysical sources anticipated to emit GWs within this range are binary white dwarfs (WDs). In fact, for a 4-year observation period, some 12,000 double white dwarfs (DWDs) are expected to be resolvable with LISA (Lamberts et al. 2019). Because the GW signals from these DWDs will be sustained for a much longer period of time than signals of a merger event, we anticipate being able to extract significant information from not only the GW frequency, but also the GW frequency "chirp," i.e., change in frequency over time ($\dot{f}$) (Shah et al. 2012).

Prospects of measuring astrophysical parameters of *detached* binary white dwarfs, in particular their individual masses, are studied in (Wolz et al. 2021). The authors express the finite-size effects of rotation and tidal effects in the binary WD gravitational waveform. They then employ universal relations between the tidal deformability and moment of inertia, and between the moment of inertia and WD mass, to express the finite-size effects in terms of the individual masses. By conducting a Fisher analysis on this waveform expressed in terms of the masses, the authors show that LISA will be able to measure the individual masses of DWDs given an initial frequency of ~ 0.02Hz and either small binary separation or relatively large masses.

In this paper, we investigate the possibility of measuring astrophysical parameters of *accreting* DWDs given LISA's measurements of the amplitude (A), frequency (f), and frequency derivative ($\dot{f}$) of GWs emanated by the DWDs. A similar analysis was carried out previously in Biscoveanu et al. (2022), where the authors use f and $\dot{f}$ to constrain the strength of tidal coupling between the binary orbit and individual WD spin, additionally paving the way for measurements of the synchronization timescale (τ_0) and a parameter indicating the binding energy of the envelope (λ). We additionally build on the work of Kaplan et al. (2012), who investigate the mass-transfer (accretion) processes and evolution of low-mass WDs that contain large hydrogen envelopes and accrete onto more massive companions. Kaplan et al. (2012) highlight the importance of understanding the relative composition of hydrogen and helium in these WDs in order to infer the stability and behavior of the binary. On the other hand, Kremer et al. (2015) study DWD systems in a colder regime, employing a cold-temperature radius approximation in their study of mass transfer and tidal effects due to asynchronicity between the binary orbit and individual WD spins. This analysis is extended in Kremer et al. (2017), which treats DWDs undergoing both direct impact and disk accretion, demonstrating how the negative chirp of these systems allows for ~ 2700 DWDs to be observable with LISA.

In this paper, we improve previous work by connecting the non-degenerate regime, in which donor WDs have the lingering hydrogen envelope discussed in Kaplan et al. (2012), with the later, degenerate regime in which the cold-temperature radius formula used by Biscoveanu et al. (2022), Kremer et al. (2015), and Kremer et al. (2017) is valid. We study the evolution of accreting DWDs through the transition between these two regimes. Knowledge of the accretion mechanism for such DWDs allows us to parameterize their gravitational waveforms in terms of the individual masses and other parameters of interest. We then perform a Fisher analysis on this waveform to determine how well we will be able to constrain the masses and other parameters given LISA's detections of GWs from accreting DWDs.

In this study, we find that with an independent measurement of the luminosity distance of our DWD systems, we are likely to be able to measure the individual masses, donor radius, and response of the donor to mass loss given LISA's measurements of the GW amplitude, frequency, and frequency derivative. Without an independent measurement of the luminosity distance, we lose our ability to constrain the individual masses, but we are still able to measure the other two parameters.

The paper is organized as follows. In Sec. 2, we introduce the parameterized gravitational waveform. In Sec. 3, we discuss how the mass-radius relations of our WDs differ in the degenerate versus non-degenerate regimes, introducing models of donors in the non-degenerate regime that we generate with a stellar evolutionary code. Sec. 4 illustrates the detectability of our DWD systems based on the relative magnitude of these systems' GW strain versus LISA's noise curve. Finally, our parameter estimation technique and results are given in Sec. 5, followed by discussion and conclusions. The geometric units of $c = G = 1$ are used in all of our equations, with the physical dimensions being recoverable through the conversion $1M_\odot = 1.5\text{km} = 4.9\times 10^{-6}\text{s}$.

2. GRAVITATIONAL WAVEFORM

The sky-averaged gravitational waveform, $h(t)$, for a DWD with donor mass m_d and accretor mass m_a is given by

$$h(t) = A\cos\phi(t). \tag{1}$$

A is the amplitude, given by

$$A = \frac{8\mathcal{M}}{5D}(\pi\mathcal{M}f)^{2/3}, \tag{2}$$

where D is the luminosity distance and $\mathcal{M}$ is the chirp mass,

$$\mathcal{M} = \frac{(m_d m_a)^{3/5}}{(m_d+m_a)^{1/5}}. \tag{3}$$

Assuming a fairly slowly changing GW frequency, so that $\ddot{f}$ and higher derivatives are negligible, the phase $\phi(t)$ is given by (Shah & Nelemans 2014)

$$\phi(t) = \phi_0 + 2\pi f_0\delta t + \pi\dot{f}_0\delta t^2, \tag{4}$$

where the subscript 0 indicates the quantity measured at the initial time of observation, t_0, and $\delta t = t - t_0$.

Examining Eqs. (2) and (4), it is evident that in order to write the waveform in terms of our parameters of interest, we must express f and $\dot{f}$ in terms of these parameters. We begin with Kepler's third law to obtain an expression for $f = 2/P_{\text{orb}}$ in terms of the masses and semi-major axis, a:

$$f = \frac{1}{\pi}\sqrt{\frac{M}{a^3}}, \tag{5}$$

where M is the total mass, $M = m_d + m_a$. The accreting DWDs we are interested in undergo mass transfer via Roche lobe overflow. In this overflow process, the donor radius, r_d, is related to a via the expression

$$a = r_d/r_L \tag{6}$$

with r_L being the Roche-lobe of the donor, given approximately as (Eggleton 1983)

$$r_L = \frac{0.49q^{2/3}}{0.6q^{2/3}+\ln(1+q^{1/3})}, \quad q = \frac{m_d}{m_a}. \tag{7}$$

In total, then, Eq. (5) gives f in terms of the two masses and the donor radius, i.e.,

$$f = \frac{1}{\pi}\sqrt{\frac{M}{(r_d/r_L)^3}}. \tag{8}$$

We differentiate Eq. (8) with respect to time to obtain an expression for $\dot{f}$ in terms of our parameters of interest. This differentiation leaves us with an $\dot{a}/a$ term that can be expressed in terms of our parameters of interest as follows.

We begin by assuming a circular orbit, giving total orbital angular momentum

$$J = m_d m_a\left(\frac{a}{M}\right)^{1/2}. \tag{9}$$

Differentiating this quantity with respect to time gives

$$\frac{\dot{J}}{J} = \frac{\dot{m}_d}{m_d}\left(1+(F-1)\frac{m_d}{m_a}-\frac{Fm_d}{2M}\right)+\frac{\dot{a}}{2a}, \tag{10}$$

The mass-loss fraction, F, defined such that $\dot{m}_a = -(1-F)\dot{m}_d$, indicates whether mass transfer is conservative or not. When $F=0$, all mass lost by the donor is gained by the accretor, and there is no overall loss of mass from the binary; when $F=1$, the accreted material is lost by the binary due to stellar winds, classical novae, etc.

We can further relate $\dot{m}_d$ and $\dot{a}$. Given Eqs. (6) and (7), it can be shown that

$$\frac{\dot{a}}{a} = \frac{\dot{m}_d}{m_d}\left[\eta_d - \zeta_{r_L}\right], \tag{11}$$

where ζ_{r_L} is the ratio between $\frac{\dot{r}_L}{r_L}$ and $\frac{\dot{m}_d}{m_d}$,

$$\begin{aligned}\zeta_{r_L} &= \frac{\dot{r}_L}{r_L}\frac{m_d}{\dot{m}_d} \\ &= \Big(q(1-F)+1\Big)\frac{2(1+q^{1/3})\ln(1+q^{1/3})-q^{1/3}}{3(1+q^{1/3})(0.6q^{2/3}+\ln(1+q^{2/3}))},\end{aligned} \tag{12}$$

and η_d is a parameter that defines the response of the donor to mass loss,

$$\eta_d = \frac{d\ln r_d}{d\ln m_d}. \tag{13}$$

If $\eta_d > 0$, the donor WD shrinks as it loses mass; if $\eta_d < 0$, as is the case for a completely degenerate WD, the donor WD's radius increases as it loses mass. With Eq. (11), we can eliminate $\dot{m}_d/m_d$ in Eq. (10) and express the total orbital angular momentum loss in terms of just $\dot{a}/a$.

On the other hand, the change in orbital angular momentum is dominated by two processes. The first of these processes is the emission of gravitational waves, which yields

$$\frac{\dot{J}_{\rm gr}}{J} = -\frac{32}{5}\frac{Mm_dm_a}{a^4}. \tag{14}$$

Angular momentum can also be lost by the binary when accreted material impacts the companion star directly, rather than forming an accretion disk around the companion. The resultant "accretion torque," which occurs at small orbits, leads to a change in angular momentum given by

$$\frac{\dot{J}_{\rm acc}}{J} = \frac{\dot{m}_d}{m_d}\sqrt{r_h\left(1+\frac{m_d}{m_a}\right)}, \tag{15}$$

where r_h is the effective radius of material orbiting the accreting companion. We use a fitting formula for r_h that depends only on the mass ratio, $q = m_d/m_a$ (Verbunt & Rappaport 1988).

When we set $\dot{J}/J = \dot{J}_{\rm gr}/J + \dot{J}_{\rm acc}/J$, we arrive at an expression for $\dot{a}/a$,

$$\frac{\dot{a}}{a} = \left(-\frac{32}{5}\frac{Mm_dm_a}{a^4}\right)\times \frac{\eta_d-\zeta_{r_L}}{1+q(F-1)-F\frac{m_d}{2m}-r_h^{1/2}(1+q)^{1/2}+\frac{\eta_d-\zeta_{r_L}}{2}}. \tag{16}$$

(In most regions of parameter space, the orbit is wide enough for an accretion disk to form; in these regions, we exclude the accretion torque term in Eq. (15), so that the quantity $-r_h^{1/2}(1+q)^{1/2}$ does not appear in the denominator of Eq. (16).) With this expression for $\frac{\dot{a}}{a}$, we can write $\dot{f}$ in terms of the parameters m_d, m_a, r_d and η_d. Revisiting Eqs. (2), (4), (8), and (16), we have a gravitational waveform in terms of the six parameters $\phi_0, m_d, m_a, r_d, \eta_d$ and D. It is this waveform that we use in our Fisher analysis to determine the measurability of each of our parameters of interest.

3. MASS-RADIUS RELATIONS

The way in which the donor WD responds to mass loss depends significantly on the composition of the donor. For cold, degenerate WDs, we can use P.P. Eggleton's analytic formula to obtain r_d in terms of m_d (Verbunt & Rappaport 1988). η_d in this cold temperature regime comes out to be about $\eta_d \sim -1/3$ for a range of m_d values.

If the donor WD is not degenerate, r_d does not vary with m_d in such a predictable manner. To reach this conclusion, we used Modules for Experiments in Stellar Astrophysics (MESA; Paxton et al. (2011)) to model mass loss from dozens of donor WDs containing a range of core and envelope masses. One of the longest lasting models we obtained is given in Fig 1. To construct this model, we used MESA to simulate the growth of a $0.153M_\odot$-helium core in the center of a pre-main sequence star. MESA then models the removal of the outer layers of hydrogen in this star via stellar winds, leaving only about $0.006M_\odot$ of a remaining hydrogen envelope. The graph of $|\eta_d|$ shown in Fig 1 begins at this point of the simulation; the initial large positive value of η_d reflects the lingering hydrogen envelope surrounding the donor WD. We then simulate mass loss from the donor, causing the WD to become increasingly degenerate as hydrogen is transferred away, resulting in a decreasing η_d function. Eventually, η_d passes through zero (seen in the cusp around $0.055M_\odot$ of stripped mass). After this point, the donor increases in size as it loses mass, causing the orbital separation of the binary to increase.

We used MESA to model many such systems, with the hope of finding patterns between the evolution of m_d and r_d that would hold for a range of core and envelope masses. This would allow us to perform a Fisher analysis on only the parameters $\theta_i = (\phi_0, m_d, m_a)$, as we could take r_d and η_d to be determined by m_d. However, the vast majority of our models reached significant numerical noise long before η_d even crossed through zero. We therefore treat r_d and η_d as unknown and include them as Fisher parameters in our parameter estimation, using the MESA model shown in Fig 1 merely to obtain fiducial r_d and η_d values as we vary m_d and m_a.

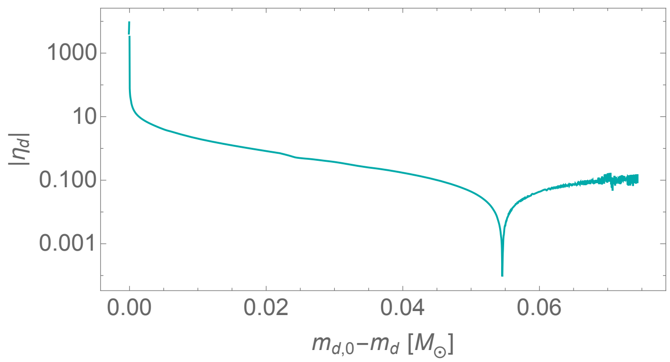

Figure 1. Plot of $|\eta_d|$ vs. stripped mass for a MESA model of a donor WD with a predominantly helium core of $0.153M_\odot$ and surrounding hydrogen envelope of $0.006M_\odot$. Numerical noise halted the model after about $0.07M_\odot$ of mass had been stripped from the donor.

4. GW STRAIN VS. LISA'S NOISE CURVE

In Fig 2, we present plots of the GW strain compared to LISA's noise curve over a range of GW frequencies. We see that in both the early (dashed) and late (solid) stages of evolution of these binaries, the GW strain (plotted as $A \times (\mathrm{T_{obs}})^{1/2}$, where $\mathrm{T_{obs}}$ is the observation time that we take to be 4 years) is several orders of magnitude higher than LISA's noise curve ($S_n(f)$; Robson et al. (2019)). This indicates that we are likely to be able to detect GW signals from the DWD systems using LISA. The dashed plots model the GW strain during an earlier stage of DWD evolution, when the donor has a significant remnant of hydrogen envelope surrounding its degenerate helium core. We construct these plots using Eqs. (2) and (8), along with the mass-radius relation from the MESA model shown in Fig 1. In this early stage of evolution, the frequency first increases, reflecting the shrinking of the binary orbit due to GW radiation. As the WDs approach each other, mass transfer is initiated, and eventually the majority of the hydrogen surrounding the donor is depleted, leaving the donor largely degenerate. This causes the donor's radius to increase as it continues losing mass, which in turn causes the orbital separation to grow (i.e., f begins to decrease again). The solid lines show the GW strain at a much later stage of evolution, when the donor is fully degenerate and f is steadily decreasing toward the bottom left-hand corner of the plot. To construct the solid-line plots, we use Eggleton's cold-temperature mass-radius formula (Verbunt & Rappaport 1988).

Fig 2 also shows a plot of the signal-to-noise ratio (SNR) at a luminosity distance of 1kpc. As an SNR of ~ 8 is generally taken as the minimum SNR for detectability, this plot confirms that LISA should be able to detect the DWDs discussed here.

5. ASTROPHYSICAL PARAMETER INFERENCE

5.1. *Fisher Method*

Given our gravitational waveform derived in Sec. 2, we can estimate the error on each of our parameters of interest using a Fisher information matrix (FIM) (Cutler 1998; Shah et al. 2012; Shah & Nelemans 2014). This method of parameter estimation assumes stationary and Gaussian detector noise.

The FIM is defined as

$$\Gamma_{ij} = \left(\frac{\partial h}{\partial \theta^i} \middle| \frac{\partial h}{\partial \theta^j} \right), \tag{17}$$

where the partial derivatives of the waveform, h, are taken with respect to the parameters of interest described in the previous section,

$$\theta^i = (\phi_0, m_d, m_a, r_d, \eta_d, D). \tag{18}$$

The inner product in Eq. (17) is given by

$$(a|b) = 4\int_0^\infty \frac{\tilde{a}^*(f)\tilde{b}(f)}{S_n(f)} df \approx \frac{2}{S_n(f_0)} \int_0^T a(t)b(t)dt\,, \tag{19}$$

with spectral noise density S_n and observation time T. Tildes indicate Fourier components, and the asterisk denotes the complex conjugate of $\tilde{a}(f)$. We take LISA's S_n from Robson et al. (2019) ($\sqrt{S_n(0.02\mathrm{Hz})} = 1.43 \times 10^{-20}\,\mathrm{Hz}^{-1/2}$). The monochromatic nature of DWD signals is assumed in our approximation, $S_n(f) \approx S_n(f_0)$, and we use Parseval's theorem to convert the inner product defined in the frequency domain to an integral in the time domain.

By inverting the FIM defined in Eq. (17), we obtain the 1-σ uncertainty on each of the parameters:

$$\Delta\theta_i = \sqrt{(\Gamma^{-1})_{ii}}. \tag{20}$$

We further impose Gaussian priors on m_d and m_a, with the priors σ_{θ^i} defined such that (Poisson & Will 1995; Cutler & Flanagan 1994; Carson & Yagi 2020)

$$\Delta\theta_i = \sqrt{(\tilde{\Gamma}^{-1})_{ii}}\,, \quad \tilde{\Gamma}_{ij} = \Gamma_{ij} + \frac{1}{\sigma^2_{\theta^i}}\delta_{ij}. \tag{21}$$

Because we are only considering DWD systems with low mass donors ($m_d \lesssim 0.2M_\odot$), we set the prior on the donor to $\sigma_{m_d} = 0.2M_\odot$. Requiring the accretor WD to have a larger

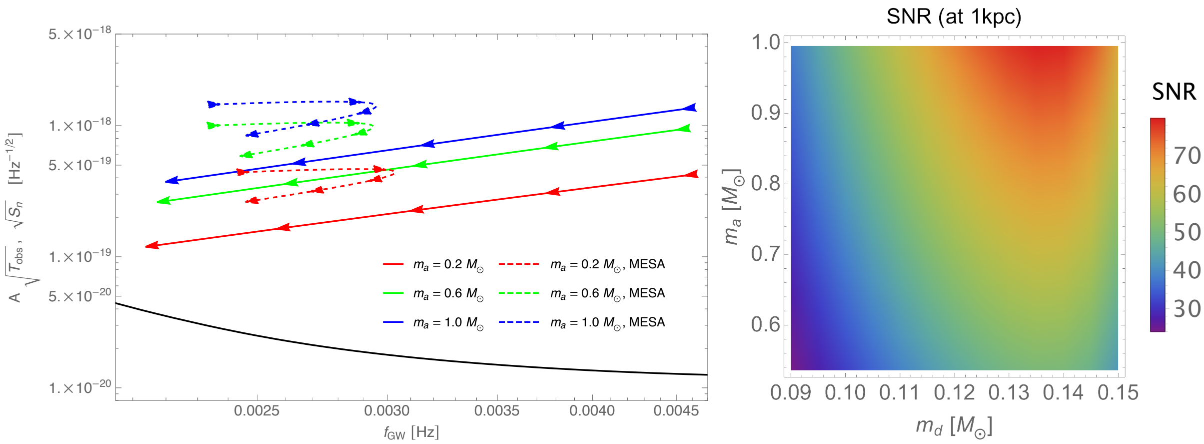

Figure 2. *Left:* GW strain $(A \times (\mathrm{T_{obs}})^{1/2}$; red, green, blue) and LISA's noise curve (black) vs. GW frequency for degenerate (solid) and non-degenerate (dashed) DWD systems at a luminosity distance of 1kpc. Arrows show the direction of evolution. The frequency ranges correspond to donor mass ranges of $0.040-0.100M_\odot$ and $0.085-0.155M_\odot$ for the solid and dashed lines, respectively. *Right:* the signal-to-noise ratio (SNR) computed for a DWD system with a donor modeled by MESA. Based on these plots, we expect GWs from the DWDs we study to be detectable at distances around 1kpc.

mass than the donor WD, we set the prior on the accretor to $\sigma_{m_a} = 0.8M_\odot$, as WDs are generally not observed with masses much higher than $\sim 1.0M_\odot$.

For fiducial values, we take $\phi_0 = 3.666$ rad and $D = 1$kpc unless otherwise stated, and vary (m_d, m_a). By virtue of the mass-radius relations introduced in Sec. 3, varying m_d also varies the parameters r_d and η_d. Our results are shown for an observation time of $\mathrm{T_{obs}} = 4$ years.

5.2. *Dynamical Stability for the DWD systems*

The mass transfer process for the DWDs considered here is expected to be unstable for certain mass ratios. Such unstable mass transfer causes dynamical instability of the binary and ultimately results in short-lived DWDs that we do not expect to observe with LISA. We follow Rappaport et al. (1982) in taking mass transfer to be stable when $\dot{m}_d < 0$. Revisiting Eqs. (11) and (16), we arrive at the following criterion for dynamical stability of the binary:

$$1 + q(F-1) - F\frac{m_d}{2m} - r_h^{1/2}(1+q)^{1/2} + \frac{\eta_d - \zeta_{r_L}}{2} > 0. \tag{22}$$

From this expression, it is evident that dynamical stability is dependent on the value of the mass-loss fraction, F. F is determined by whether or not the accreted material can be burned stably. We take the criterion for stable hydrogen burning from Kaplan et al. (2012). This criterion, which takes into account the reduced metallicity of the accreting WD, is $\dot{m} > 10^{-7}(m_a/M_\odot - 0.5357)M_\odot \mathrm{yr}^{-1}$. For mass transfer rates lower than this, we assume unstable hydrogen burning and set $F = 1$. For mass transfer rates above the critical mass loss rate, we assume stable hydrogen burning and set $F = 0$.

As mentioned previously, there are large regions of parameter space in which the orbit is wide enough for an accretion disk to form. In such cases, we again exclude the accretion torque term $-r_h^{1/2}(1+q)^{1/2}$, leading to greater dynamical stability (i.e., more regions in which the left-hand side of Eq. (22) is greater than zero).

5.3. *Results: Gravitational-wave Observations Alone*

We now present the results of our Fisher analysis that we obtain if there is no way to independently constrain the luminosity distance, D. In this case, we include D in our parameter set:

$$\theta^i = (\phi_0, m_d, m_a, r_d, \eta_d, D) \tag{23}$$

Plots of the error on the parameters η_d, r_d, and D are given in Fig 3. Unfortunately, in this case, we find that our Fisher analysis merely returns the priors we impose on the masses, i.e., we gain no additional constraints on the individual masses of the donor and accretor WDs.

Although we appear to be unable to constrain the individual masses without an independent measurement of D, there are large regions of parameter space in which the fractional error on r_d is smaller than is required for the measurability threshold, $\Delta r_d / r_d = 1$. The same cannot be said for D; our Fisher analysis does not assist us in constraining the luminosity distance.

For η_d, we plot just the error rather than the fractional error because the smallness of η_d itself as the donor WD becomes degenerate causes the fractional error on this parameter to be very large, giving a false sense of an inability to constrain the parameter. In reality, there is a large region of the parameter space in which the error on η_d is very small. In the plot of $\Delta\eta_d$, we see a discontinuity around $m_a \approx 0.6M_\odot$. This line separates the region of parameter space in which the mass loss fraction, F, equals 0 (lower portion of the plot) from the region in which $F = 1$ (upper portion). In other words,

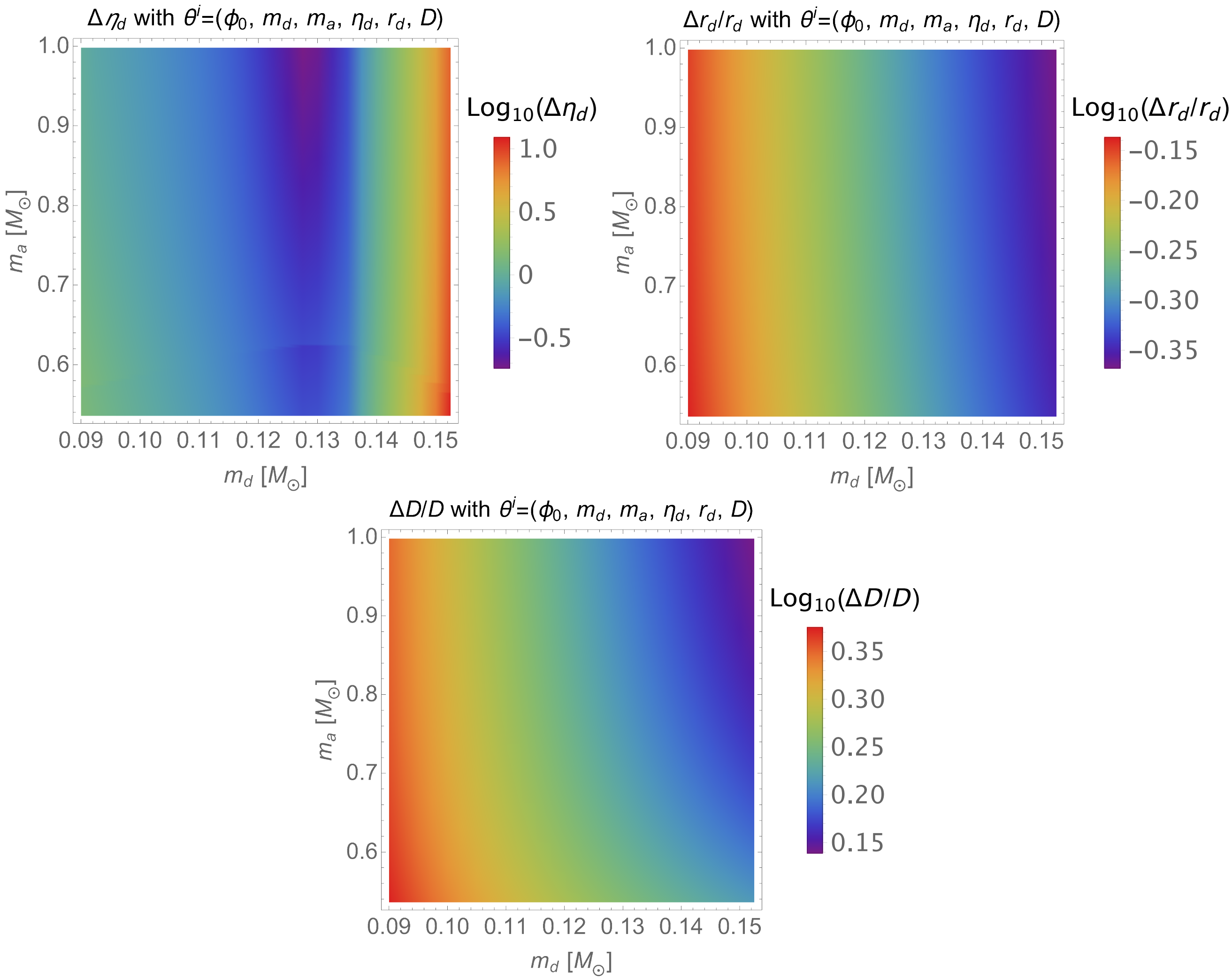

Figure 3. Error on η_d and fractional error on r_d and D, calculated via our Fisher analysis including D as a Fisher parameter. Since inverting the FIM merely returns the priors on the individual masses, giving no new constraints on the mass values, we do not show plots for these parameters.

accreted hydrogen burns stably on the accreting companion only in the lower region of parameter space.

In general, we find that the fractional error on r_d (excluding correlations between parameters) scales with the signal-to-noise ratio (SNR) times $\frac{df}{dr_d} \times r_d$. This is intuitive; we see from Eq. (8) that f depends significantly on r_d through the orbital separation, and the error should of course decrease with a larger SNR. The extra factor of r_d accounts for the fact that want to compare the derivative against our plots of fractional error (i.e., Δr_d divided by a factor of r_d). In a similar manner, we find that the error on η_d scales with SNR $\times \frac{d\dot{f}}{d\eta_d}$, which is sensible, as η_d only appears in $\dot{f}$ and not the amplitude or other parts of the phase. Finally, we find that the error on D scales with SNR $\times \frac{dA}{dD} \times D$. This is also as we expect; the only place luminosity distance appears in our parameterized gravitational waveform is through the amplitude (Eq. (2)). For plots and more discussion on the scaling of parameter error with various derivatives of the waveform, see App. B.

To summarize, in the absence of an electromagnetic counterpart to LISA's measurements of accreting DWDs, our Fisher analysis suggests that we will only likely be able to constrain r_d and possibly η_d out of the six parameters appearing in our gravitational waveform.

5.4. *Results: Gravitational-wave Observations with Electromagnetic Counterparts*

A recent paper has shown that at least ~ 60 DWDs with helium-rich donors are expected to be observable by both LISA and GAIA (Breivik et al. 2018). For these DWD systems, we can obtain an independent measurement of the luminosity distance, D, from GAIA. This reduces the number of unknown parameters by one, leaving us with the parameter set

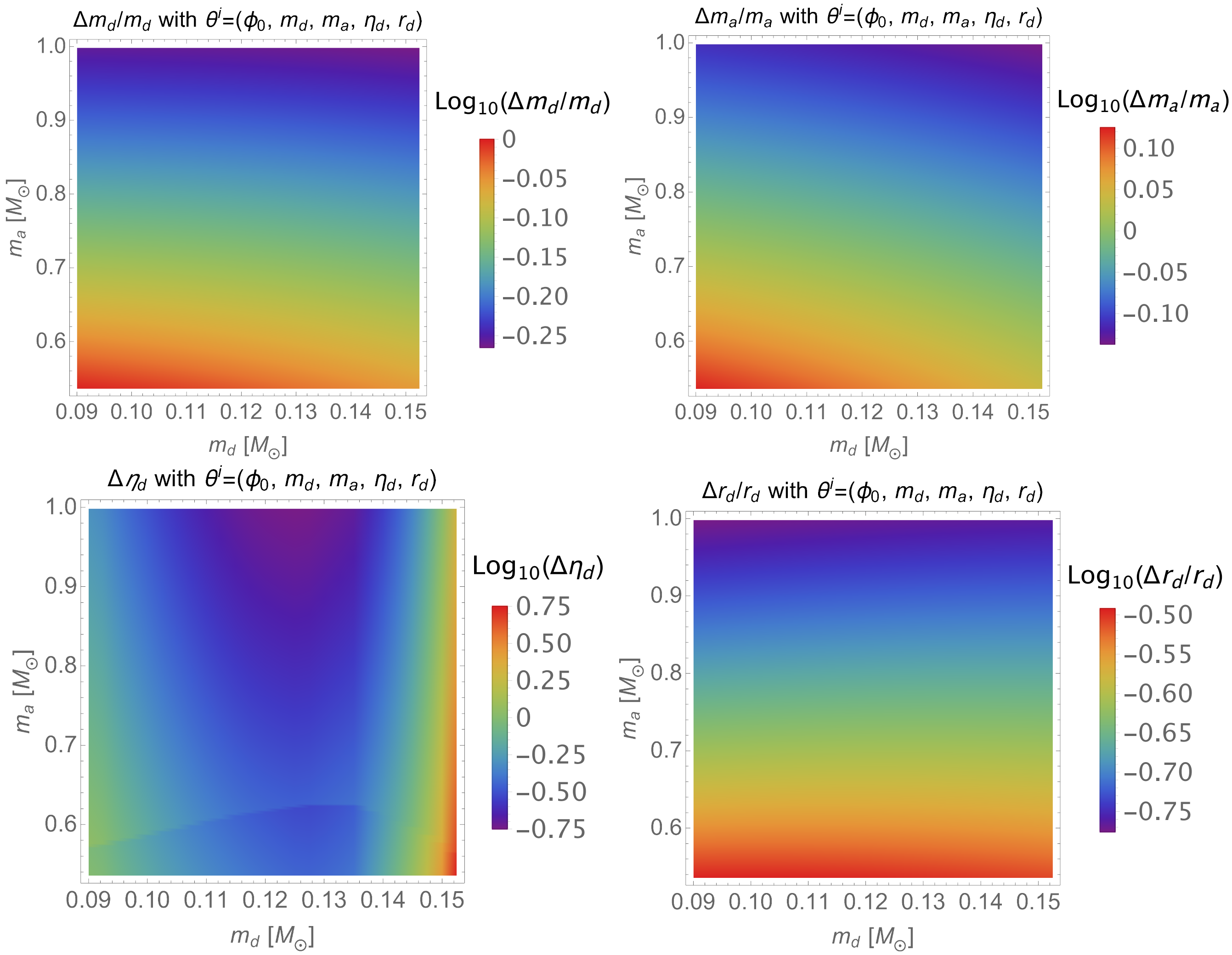

Figure 4. *Top row:* Fractional error on the individual masses as determined via Fisher analysis. *Bottom row, left to right:* Error on η_d and fractional error on r_d given by the Fisher analysis. Fiducial values for η_d and r_d were obtained from the MESA mass-radius relation given in Fig 1.

$$\theta^i = (\phi_0, m_d, m_a, r_d, \eta_d). \tag{24}$$

It turns out that our ability to constrain the individual masses of accreting DWD systems is considerably enhanced if we do not need to include D as a Fisher parameter.

Figure 4 shows the measurement uncertainties calculated for the parameters m_d, m_a, η_d, and r_d, as determined via Fisher analysis excluding D as a parameter. In total, we see that if we have an independent measurement of D, we can anticipate being able to constrain each of our parameters of interest, including m_d and m_a, which we were unable to do without the complementary measurement of D. The measurability of r_d is also considerably enhanced when we perform the Fisher analysis on only five parameters.

Once again, we find that the error (without correlations) on r_d and η_d scale with SNR $\times \frac{df}{dr_d} \times r_d$ and SNR $\times \frac{d\dot{f}}{d\eta_d}$, respectively. The errors on m_d and m_a do not follow such a simple scaling because of the additional priors that we impose on these parameters. Instead, we find that the error on m_a is mainly dominated by the prior with a slight improvement that comes from the amplitude. On the other hand, the error on m_d is determined both from the amplitude and phase.

For the results shown in both Sec. 5.3 and Sec 5.4, we note that the error on m_d, m_a, and r_d does not change significantly when we use different mass-radius relations for fiducial values of r_d and η_d. The error on η_d decreases by almost two orders of magnitude when we use Eggleton's cold-temperature mass-radius relation instead of a MESA model for fiducial values.

We also note that although the error without correlations increases by an order of magnitude when we study DWD systems at 10kpc instead of 1kpc, the full error on m_d, m_a, and r_d is heavily dependent enough upon the priors and upon correlations between parameters to not change significantly when we increase the fiducial luminosity distance to 10kpc. The error on η_d, on the other hand, increases by a little over an order of magnitude. At 10kpc, the SNR plotted in Fig 2 decreases by a factor of 10, so that there is only a small region of parameter space (red region of the plot) in which GWs from DWD systems should be above the detectability threshold (SNR~ 8).

6. CONCLUSIONS

We parameterize the GWs that we expect LISA to detect from accreting DWD systems in terms of the parameters $\theta_i = (\phi_0, m_d, m_a, \eta_d, r_d, D)$. We perform a Fisher analysis on the parameterized waveform, imposing Gaussian priors on the individual masses based on properties of the DWDs we expect to be generating the GWs. We find from our Fisher analysis that if we can obtain simultaneous, independent measurements of D (from a separate detector like GAIA), then we are likely to be able to constrain not only the individual masses, m_d and m_a, but also the parameters η_d and r_d. However, if we do not have an independent measurement of D, then although our Fisher analysis still reveals reasonable measurability of η_d and r_d, we lose our ability to constrain the individual masses. For future work, it would be interesting to confirm and generalize our findings using a full Bayesian Markov-chain Monte-Carlo analysis (Cornish & Littenberg 2007).

ACKNOWLEDGMENTS

We all thank the support by NASA Grant No.80NSSC20K0523. S. Y. would like to also thank the UVA Harrison Undergraduate Research Award and the Virginia Space Grant Consortium Undergraduate Research Scholarship Award No.AWD-001682.

APPENDIX

A. CORROBORATION OF THE $M_D - F$ RELATION FOR NEGATIVELY CHIRPING DWD SYSTEMS

In a previous work, Breivik et al. (2018) report nearly identical evolutionary tracks of m_d versus f in their simulations of several thousand negatively chirping DWDs containing low-mass helium core donors. They fit the relation between m_d and f to a fourth-order polynomial shown in Fig 5. In the same figure, we plot tracks of m_d versus f calculated via Eq. 8, using Eggleton's cold-temperature mass-radius relation to obtain donor radius values (Verbunt & Rappaport 1988). It is evident that despite the accretor mass appearing in the total mass in Eq. 8, the evolution of f with m_d is largely insensitive to the mass of the accreting companion in the negatively chirping (i.e., cold temperature) regime. For DWDs containing low-mass degenerate donors, our analytic calculation of f agrees excellently with the analytic fit in Eq. (1) of Verbunt & Rappaport (1988).

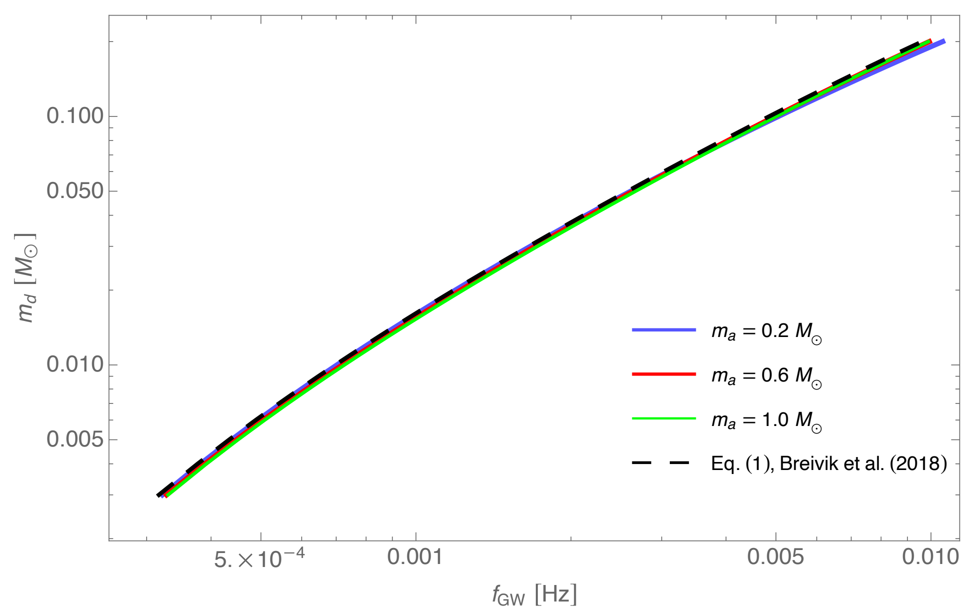

Figure 5. Our evolutionary tracks of m_d vs. f for low-mass degenerate WDs, plotted against the analytic fit for similar DWD systems studied in Verbunt & Rappaport (1988).

B. IDENTIFICATION OF PARAMETER ERROR WITH DIFFERENT PIECES OF THE WAVEFORM

In Sec. 5.3 and Sec. 5.4, we mention the scaling of the error on r_d and η_d with the SNR times df/dr_d and $d\dot{f}/d\eta_d$, respectively. In Sec. 5.3, we additionally find that the error on D scales with SNR$\times dA/dD$. To illustrate this point, we plot the error on each of these parameters (without correlations) alongside the partial derivative of the waveform with which the error scales. We show plots for just the six-parameter case (i.e., including D as a Fisher parameter), as the scaling of the error on η_d and r_d works much the same way for both the five- and six-parameter cases.

Based on Fig 6, we see that r_d is largely determined by f, η_d is determined by $\dot{f}$, and D is determined by A. The latter two statements are not surprising; η_d and D only appear in the waveform through $\dot{f}$ and A, respectively, so we would not expect the error on these parameters to be affected by anything else (other than the SNR). The clear scaling of r_d with f is slightly less trivial, since r_d technically appears in all three pieces of the waveform, A, f, and $\dot{f}$. However, since r_d only enters the amplitude and $\dot{f}$ through f, we should not ultimately be surprised that r_d scales most strongly with just the GW frequency (and SNR).

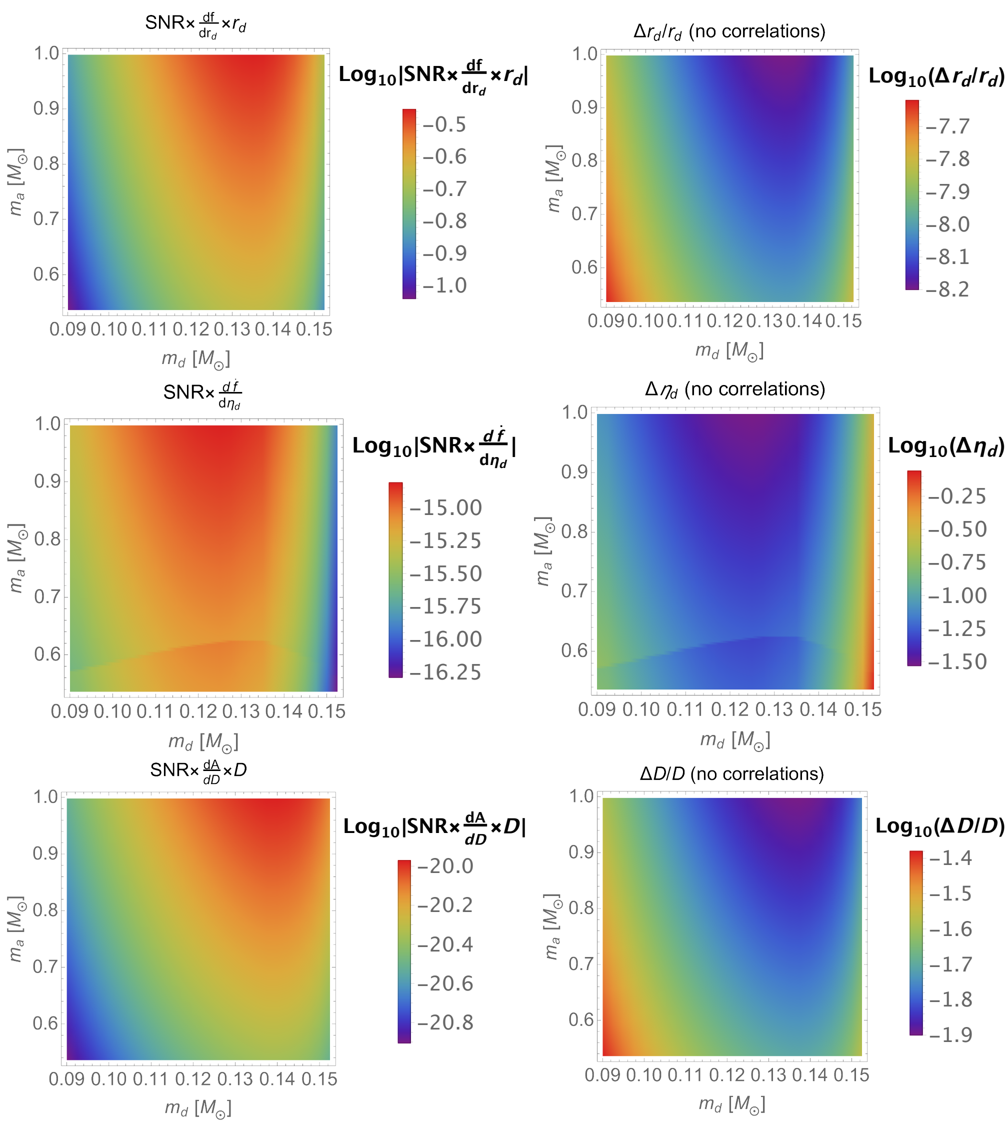

Figure 6. Plots showing how the error on r_d, η_d, and D is determined by different pieces of the waveform.

REFERENCES

Abbott, B. P., et al. 2016, Phys. Rev. Lett., 116, 061102, doi: 10.1103/PhysRevLett.116.061102

—. 2017, Phys. Rev. Lett., 119, 161101, doi: 10.1103/PhysRevLett.119.161101

—. 2019, Phys. Rev., X9, 031040, doi: 10.1103/PhysRevX.9.031040

Abbott, R., et al. 2021, Astrophys. J. Lett., 915, L5, doi: 10.3847/2041-8213/ac082e

Amaro-Seoane, P., et al. 2017. https://arxiv.org/abs/1702.00786

Biscoveanu, S., Kremer, K., & Thrane, E. 2022, arXiv e-prints, arXiv:2206.15390, doi: 10.48550/arXiv.2206.15390

Breivik, K., Kremer, K., Bueno, M., et al. 2018, Astrophys. J. Lett., 854, L1, doi: 10.3847/2041-8213/aaaa23

Carson, Z., & Yagi, K. 2020, Phys. Rev., D101, 044047, doi: 10.1103/PhysRevD.101.044047

Cornish, N. J., & Littenberg, T. B. 2007, Phys. Rev., D76, 083006, doi: 10.1103/PhysRevD.76.083006

Cutler, C. 1998, Phys. Rev., D57, 7089, doi: 10.1103/PhysRevD.57.7089

Cutler, C., & Flanagan, É. E. 1994, PhRvD, 49, 2658, doi: 10.1103/PhysRevD.49.2658

Eggleton, P. P. 1983, Astrophys. J., 268, 368, doi: 10.1086/160960

Kaplan, D. L., Bildsten, L., & Steinfadt, J. D. R. 2012, Astrophys. J., 758, 64, doi: 10.1088/0004-637X/758/1/64

Kremer, K., Breivik, K., Larson, S. L., & Kalogera, V. 2017, ApJ, 846, 95, doi: 10.3847/1538-4357/aa8557

Kremer, K., Sepinsky, J., & Kalogera, V. 2015, ApJ, 806, 76, doi: 10.1088/0004-637X/806/1/76

Lamberts, A., Blunt, S., Littenberg, T. B., et al. 2019, Mon. Not. Roy. Astron. Soc., 490, 5888, doi: 10.1093/mnras/stz2834

Paxton, B., Bildsten, L., Dotter, A., et al. 2011, Astrophys. J. Suppl., 192, 3, doi: 10.1088/0067-0049/192/1/3

Poisson, E., & Will, C. M. 1995, Phys. Rev., D52, 848, doi: 10.1103/PhysRevD.52.848

Rappaport, S., Joss, P., & Webbink, R. 1982, Astrophys. J., 254, 616, doi: 10.1086/159772

Robson, T., Cornish, N. J., & Liu, C. 2019, Class. Quant. Grav., 36, 105011, doi: 10.1088/1361-6382/ab1101

Shah, S., & Nelemans, G. 2014, Astrophys. J., 791, 76, doi: 10.1088/0004-637X/791/2/76

Shah, S., van der Sluys, M., & Nelemans, G. 2012, A&A, 544, A153, doi: 10.1051/0004-6361/201219309

Verbunt, F., & Rappaport, S. 1988, Astrophys. J., 332, 193, doi: 10.1086/166645

Wolz, A., Yagi, K., Anderson, N., & Taylor, A. J. 2021, MNRAS, 500, L52, doi: 10.1093/mnrasl/slaa183